# Phenylglyoxal inhibition of the mitochondrial $F_1F_O$-ATPase activated by $Mg^{2+}$ or by $Ca^{2+}$ provides clues on the mitochondrial permeability transition pore

Cristina Algieri, Fabiana Trombetti, Alessandra Pagliarani*, Vittoria Ventrella, Salvatore Nesci

Department of Veterinary Medical Sciences; University of Bologna; Ozzano Emilia Via Tolara di Sopra 50, Bologna, 40064; Italy

*Corresponding author: alessandra.pagliarani@unibo.it Department of Veterinary Medical Sciences, University of Bologna, via Tolara di Sopra 50, 40064 Ozzano Emilia (Bologna), Italy

## Abstract

Phenylglyoxal (PGO), known to cause post-translational modifications of Arg residues, was used to highlight the role of arginine residues of the $F_1F_O$-ATPase, which may be crucial to yield ~~for~~ the mitochondrial permeability transition pore (mPTP). In swine heart mitochondria PGO inhibits ATP hydrolysis by the $F_1F_O$-ATPase either sustained by the natural cofactor $Mg^{2+}$ or by $Ca^{2+}$ by a similar uncompetitive inhibition mechanism, namely the tertiary complex (*ESI*) only forms when the ATP substrate is already bound to the enzyme, and with similar strength, as shown by the similar *K*'i values (0.82±0.07 mM in presence of $Mg^{2+}$ and 0.64±0.05 mM in the presence of $Ca^{2+}$). Multiple inhibitor analysis indicates that features of the $F_1$ catalytic sites and/or the $F_O$ proton binding sites are apparently unaffected by PGO. However, PGO and $F_1$ or $F_O$ inhibitors can bind the enzyme combine simultaneously. However they mutually hinder to bind the $Mg^{2+}$-activated $F_1F_O$-ATPase, whereas they do not mutually exclude to bind ~~for~~ the $Ca^{2+}$-activated $F_1F_O$-ATPase. The putative formation of PGO-arginine adducts, and the consequent spatial rearrangement in the enzyme structure, inhibits the $F_1F_O$-ATPase activity but, as shown by the calcium retention capacity evaluation in intact mitochondria, apparently favours the mPTP formation.

Keywords: phenylglyoxal; $F_1F_O$-ATPase; mitochondria; permeability transition pore; inhibition kinetics; divalent cations.

Abbreviations: PGO, phenylglyoxal; PTP, permeability transition pore; DCCD, dicyclohexylcarbodiimide; IMM, inner mitochondrial membrane; $\Delta\mu_{H+}$, electrochemical gradient of $H^+$; CRC, calcium retention capacity; mPTP, mitochondrial permeability transition pore.

# 1. Introduction

Chemical modifications in the side chain of critical aminoacids often cause substantial changes in enzyme structure and function. The basic aminoacid arginine has a crucial role in the functioning of bacterial and eukaryotic $F_1F_O$-ATPase [1,2], the enzyme complex which builds and hydrolyzes ATP. Other than in the enzymatic catalysis driven by the electrochemical transmembrane gradient of $H^+$ ($\Delta\mu_{H+}$) [3] and in the morphology of the *cristae* [4], most likely the enzyme complex is also involved in the formation of the mitochondrial permeability transition pore (mPTP) [10-12], which leads to mitochondrial membrane permeabilization, mitochondrial dysfunction and cell death. Interestingly, distinct arginine residues seem to be crucial to allow both the vital enzyme role as ATP builder and its lethal function in mPTP formation [1,5,6].

The $F_1F_O$-ATPase complex works by matching two rotary motors featured by different roles and structures. The hydrophilic $F_1$ domain, formed by $\alpha_3$, $\beta_3$, γ, δ, and ε subunits, sustains catalysis, namely it synthesizes or hydrolyzes ATP by its $\alpha_3\beta_3$ globular hexamer. The hydrophobic $F_O$ domain, embedded in the IMM and hosting the $H^+$ channel, consists of *a* subunit, the transmembrane α-helices of *b* subunit and the $c_8$ subunits which form the *c*-ring. Mammalian $F_1F_O$-ATPases also contain the supernumerary subunits *e*, *f*, *g*, *k*, DAPIT, 6.8 KDa proteolipid, and A6L subunits. The two domains are joined by a central stalk (composed by γ, δ, ε subunits) and a peripheral stalk, consisting of *d*, OSCP, F6 and the extrinsic α-helices of A6L and *b* subunits, which prevents the $\alpha_3\beta_3$ head rotation with $F_O$ [7]. The bi-functional $F_1F_O$-ATPase can synthesize ATP by dissipating the $\Delta\mu_{H+}$ or act *in reverse* by hydrolysing ATP and re-energize the IMM [8]. Each α/β subunit interface forms a catalytic site which undergoes one of the three conformations $\beta_{TP}$, $\beta_{DP}$ (which bind ATP with decreasing affinity) and $\beta_E$ (empty), which interconvert each other when the central stalk rotates [9]. The $F_O$ domain can channel $H^+$ across the IMM in two opposite directions, namely from the intermembrane space to the IMM and *vice versa*. Two discontinuous and asymmetric half-channels separated by a conserved Arg on *a* subunit [1] match $H^+$ flow to rotation: counterclockwise (viewed from the mitochondrial matrix side) leading to ATP synthesis, driven by downhill $H^+$ flux, and clockwise leading to ATP hydrolysis, which sustains $H^+$ pumping in the intermembrane space [10].

Mammalian $F_1F_O$-ATPases can dimerize by joining two adjacent $F_O$ domains. The *g*/*f* subunit on one side and the DAPIT/*k* subunit on the other side of the $F_1F_O$-ATPase monomer establish two dimerization contact sites with the *k*/DAPIT and *f*/*g* pairs of adjacent monomers. Moreover, two specific "curved domains" composed by the *e*, *g* subunits and the membrane N-terminal helix of *b* subunits from the two monomers form the V-shaped dimer [7,11]. These membrane subunits are involved in the $F_1F_O$-ATPase dimerization, in the formation of the *cristae* [12] and also in the $Ca^{2+}$-dependent high-conductance mPTP formation in the IMM [13], all events most likely interconnected [12].

The recent $F_1F_O$-ATPase involvement in the mPTP [14–16], in spite of some controversies [17], is especially attractive, since the mPTP dysregulation is involved in severe pathologies [18] and in aging [19]. By making the IMM unselective to small solutes (less than 1.5 KDa), the mPTP and its long-lasting openings can trigger cell death. The mPTP channel would form between the $F_1F_O$-ATPase monomers of the dimer [14] or alternatively within the *c*-ring [15,16], as *c* subunit ablation reduced the mPTP conductance [20]. Recently, a tight connection between the mPTP and the mitochondrial $Ca^{2+}$-activated $F_1F_O$-ATPase activity was proven in our lab [21], which sustains the hypothesis that the $Ca^{2+}$-dependent F-ATPase activity would open the mPTP through a conformational mechanism [21].

Phenylglyoxal (PGO), long known to react preferentially with the guanidino group of arginine [22], is widely exploited as chemical tool, not only to explore the role of arginine residues in the mitochondrial $F_1F_O$-ATPase function, but also to cast light in the mechanisms of mPTP formation in which arginine is thought to be involved [6]. PGO, which contains both an aldehyde and a ketone group, is chemically reactive, while its phenyl head allows incorporation in hydrophobic environments. The guanidino group of arginine, which

makes it the most basic aminoacid in proteins and a poor nucleophile, can react with PGO to produce multiple products whose identification is still a challenge. Consistently, the species-dependent PGO effects on the mPTP were related to the different adducts established within the enzyme structure [6,23–25].

On these bases, the present study exploits PGO to verify if the likely formation of stable adducts with the $F_1F_O$-ATPase Arg residues modifies the F-ATPase activity, stimulated by either the natural cofactor $Mg^{2+}$ or by $Ca^{2+}$, and affects PTP opening. The mechanisms yielding mPTP formation, investigated in this work, may hopefully be exploited to counteract the deleterious effects of mPTP dysregulation.

# 2. Material and methods

## 2.1. Chemicals

Sodium azide, dicyclohexylcarbodiimide (DCCD) and oligomycin were purchased by Vinci-Biochem (Vinci, Italy). $Na_2ATP$ and phenylglyoxal were obtained from Sigma–Aldrich (Milan, Italy). All other chemicals were reagent grade. Quartz double distilled water was used for all reagent solutions except when differently stated.

## 2.2. Preparation of the mitochondrial fractions

Swine hearts (*Sus scrofa domesticus*) were collected at a local abattoir and transported to the lab within 2 h in ice buckets at 0–4°C. After removal of fat and blood clots as much as possible, approximately 30–40 g of heart tissue were rinsed in ice-cold washing Tris-HCl buffer (medium A) consisting of 0.25 M sucrose, 10 mM Tris(hydroxymethyl)-aminomethane (Tris), pH 7.4 and finely chopped into fine pieces with scissors. Each preparation was made from one heart. Once rinsed, tissues were gently dried on blotting paper and weighted. Then tissues were homogenized in a buffer (medium B) consisting of 0.25 M sucrose, 10 mM Tris, 1 mM EDTA (free acid), 0.5 mg/mL BSA fatty acid free, pH 7.4 with HCl at a ratio of 10 mL medium B per 1 g of fresh tissue. After a preliminary gentle break up by Ultraturrax T25, the tissue was carefully homogenized by a motor-driven teflon pestle homogenizer (Braun Melsungen Type 853202) at 650 rpm with 3 up-and-down strokes. The mitochondrial fraction was then obtained by stepwise centrifugation (Sorvall RC2-B, rotor SS34). Briefly, the homogenate was centrifuged at 1,000 *g* for 5 min, thus yielding a supernatant and a pellet. The pellet was re-homogenized under the same conditions of the first homogenization and re-centrifuged at 1,000 *g* for 5 min. The gathered supernatants from these two centrifugations, filtered through four cotton gauze layers, were centrifuged at 10,500 *g* for 10 min to yield the raw mitochondrial pellet. The raw pellet was resuspended in medium A and further centrifuged at 10,500 *g* for 10 min to obtain the final mitochondrial pellet. The latter was resuspended by gentle stirring using a Teflon Potter Elvejehm homogenizer in a small volume of medium A, thus obtaining a protein concentration of 30 mg/mL [26]. All steps were carried out at 0–4°C. The protein concentration was determined according to the colorimetric method of Bradford [27] by Bio-Rad Protein Assay kit II with BSA as standard. The mitochondrial preparations were then stored in liquid nitrogen until the evaluation of F-ATPase activities.

## 2.3. Mitochondrial F-ATPase activity assays

Immediately after thawing, mitochondrial preparations were used for F-ATPase activity assays. The capability of ATP hydrolysis was assayed in a reaction medium (1 mL) containing 0.15 mg mitochondrial

protein and 75 mM ethanolammine–HCl buffer pH 9.0, 6.0 mM $Na_2ATP$ and 2.0 mM $MgCl_2$ for the $Mg^{2+}$-activated $F_1F_O$-ATPase assay, and a the same buffer at pH 8.8 plus 3.0 mM $Na_2ATP$ and 2.0 mM $CaCl_2$ for the $Ca^{2+}$-activated $F_1F_O$-ATPase assay. After 5 min preincubation at 37°C, the reaction, carried out at the same temperature, was started by the addition of the substrate $Na_2ATP$ and stopped after 5 min by the addition of 1 mL of ice-cold 15% (w/w) trichloroacetic acid aqueous solution. Once the reaction was stopped, vials were centrifuged for 15 min at 3,500 rpm (Eppendorf Centrifuge 5202). In the supernatant, the concentration of inorganic phosphate (Pi) hydrolyzed by known amounts of mitochondrial protein, which is an indirect measure of F-ATPase activity, was spectrophotometrically evaluated [28]. To this aim, 1 µL from a mother solution of 3 mg/mL oligomycin in dimethylsulfoxide was directly added to the reaction mixture before starting the reaction. The total ATPase activity was calculated by detecting the Pi in control tubes run in parallel and containing 1 µL dimethylsulfoxide per mL reaction system. In each experimental set, control tubes were alternated to the condition to be tested. The employed dose of oligomycin, specific inhibitor of F-ATPase which selectively blocks the $F_O$ subunit ensured maximal enzyme activity inhibition and was currently used in F-ATPase assays [21]. The $F_1F_O$-ATPase activity was routinely measured by subtracting, from the Pi hydrolyzed by total ATPase activity, the Pi hydrolyzed in the presence of oligomycin [26]. In all experiments the F-ATPase activity was expressed as µmol Pi·mg protein$^{-1}$·min$^{-1}$.

## 2.4. Kinetic analyses

To calculate the $IC_{50}$ values, namely the inhibitor concentration which causes half maximal inhibition of the enzyme activity, the enzyme activity data obtained in the absence of PGO and in the presence of increasing PGO concentrations where used to calculate the enzyme inhibition that, after background correction, were fitted to a 3 parameter equation (*i*), where the lower data limit (no enzyme inhibition) is 0. In equation (*i*) the enzyme activity (*y*) is a function of the inhibitor concentration (*x*), "*Range*" is the uninhibited enzyme activity (in absence of inhibitor), and *s* is a slope factor. As *x* is at the denominator, *y* falls at increasing *x* values.

$$y = \frac{Range}{1+(\frac{x}{IC_{50}})^s} \qquad (i)$$

The graphical methods of Dixon and Cornish-Bowden plots, which complement one another [29], were used to detect the inhibition mechanism of PGO on the $Ca^{2+}$- or $Mg^{2+}$-activated $F_1F_O$-ATPase. The 1/*v* (reciprocal of the enzyme activity) in Dixon plot or the S/*v* ratio in Cornish-Bowden plot were plotted as a function of the PGO concentration. To build these plots, different experimental sets were designed in which the F-ATPase activity was evaluated in the presence of increasing PGO concentrations at two ATP concentrations, keeping the metal cofactor concentration constant. The values of $K'_i$, which represent the dissociation constant of the ternary *ESI* complex, were calculated as the abscissa (changed to positive) of the intercept of the straight lines obtained in the Cornish-Bowden plots. In all plots the enzyme specific activity was taken as the expression of *v*.

Kinetic studies on the mutual exclusion of different inhibitors on the same F-ATPase activity were carried out. These analyses aimed at casting light on the possible interaction on $F_1$ domain between PGO and azide, a known $F_1$ inhibitor and on $F_O$ domain between PGO and either oligomycin or DCCD, both known $F_O$ inhibitors. To build Dixon-like plots, in which the reciprocal of enzyme activity data (1/*v*) (*y* axis) were plotted versus PGO concentration (*x* axis), the F-ATPase activity was assayed in the presence of increasing PGO concentrations at fixed concentrations of $F_1$ or $F_O$ inhibitor and at constant ATP substrate concentration. According to the graphical method employed [30], when the straight lines show different slopes and intersection points, the enzyme inhibition mirrors the combined effect of the two inhibitors. When the F-ATPase is inhibited by two not mutually exclusive compounds, for instance PGO ($I_1$) plus $F_1$ inhibitor ($I_2$) or PGO ($I_1$) plus $F_O$ inhibitor ($I_2$), the enzyme can combine with both inhibitors yielding the

quaternary complex $ESI_1I_2$ [31]. The value of $-\alpha K'_i$, which represents the dissociation constant of the quaternary $ESI_1I_2$ complex, was calculated from the abscissa (changed to positive) of the point of intersection of the two straight lines obtained in the presence and absence of $F_1$ or $F_O$ inhibitor. The interaction constant α was then calculated from the ratio of ~~between~~ $\alpha K'_i$ ~~and~~ to $K'_i$ [31] (Table 2).

All data were processed by GraFit Data Analysis Software (version 7.0.3). The correlation coefficients of all the straight lines obtained in Dixon and Cornish Bowden plots were never lower than 0.95, thus confirming the linearity of these plots.

### 2.5. mPTP evaluation

Immediately after the preparation of swine heart mitochondrial fractions, mitochondria (1mg/mL) were suspended and energized in the assay buffer (130 mM KCl, 1 mM $KH_2PO_4$, 20 mM HEPES, pH 7.2 with TRIS), incubated at 25°C with 1 μg/mL rotenone and 5 mM succinate as respiratory substrate. To evaluate PGO effect, selected PGO doses were added to mitochondrial suspensions prior to PTP evaluation. PTP opening was induced by the addition of ~~small~~ low concentrations of $Ca^{2+}$ (10 μM) as $CaCl_2$ solution at fixed time intervals (1 min). The calcium retention capacity (CRC) was spectrofluorophotometrically evaluated in the presence of 0.8 μM Fura-FF. The probe has different spectral properties in the absence and in the presence of $Ca^{2+}$, namely it displays excitation/emission spectra of 365/514 nm in the absence of $Ca^{2+}$ (Fura-FF low $Ca^{2+}$) and shifts to 339/507 nm in the presence of high $Ca^{2+}$ concentrations (Fura-FF high $Ca^{2+}$). mPTP opening, which implies a decrease in CRC, was detected by the increase in the fluorescence intensity ratio (Fura-FF high $Ca^{2+}$)/(Fura-FF low $Ca^{2+}$). All measurements were processed by LabSolutions RF software [21].

### 2.6. Statistical Analysis

The data represent the mean ± SD (shown as vertical bars in the figures) of the number of experiments reported in the figure captions and table legends. In each experimental set, the analyses were carried out on different pools of animals. The differences between the enzyme activity data in differently treated mitochondria were evaluated by one way ANOVA followed by Dunnett test when *F* values indicated significance ($P \leq 0.05$).

## 3. Results

### 3.1. PGO effect on the $Ca^{2+}$- and $Mg^{2+}$-activated $F_1F_O$-ATPase activities

Apparently, the $Ca^{2+}$- and $Mg^{2+}$-activated $F_1F_O$-ATPases are similarly inhibited by PGO, which exerts the same magnitude order of the inhibition extent, being the maximal enzyme inhibition attained at approximately 4 mM PGO in both cases (Fig. 1). However, on considering the $IC_{50}$ values, PGO inhibits much more strikingly the $Ca^{2+}$-dependent F-ATPase ($IC_{50}$= 0.52±0.05 mM) that the $Mg^{2+}$-dependent F-ATPase ($IC_{50}$= 1.10±0.07 mM) (Fig. 1). The inhibition mechanism of PGO on both the $Ca^{2+}$- and $Mg^{2+}$-activated $F_1F_O$-ATPases is uncompetitive with respect to the ATP substrate (Fig. 2A-B,C-D), namely PGO can only bind to the enzyme-ATP (*ES*) complex forming the tertiary complex (*ESI*), irrespective of the divalent cation which acts as cofactor. Moreover, the Cornish-Bowden plots show that the dissociation constant of the *ESI* complex ($K'_i$) of the $Ca^{2+}$-activated $F_1F_O$-ATPase is lower (0.64±0.05 mM) (Fig. 2B) than that of the $Mg^{2+}$-activated $F_1F_O$-ATPase (0.82±0.07 mM) (Fig. 2D), thus indicating that in the presence of $Ca^{2+}$ the formation of the ternary complex is easier and stronger than in the presence of $Mg^{2+}$.

### 3.2. PGO and inhibitors of $F_1$ and $F_O$ domain in multiple inhibition analysis

Mutual exclusion analyses, carried out by incorporating binary mixtures of $F_1$ and $F_O$ inhibitors to the F-ATPase reaction media, aimed at verifying the possible interaction of PGO with the catalytic sites of the hydrophilic $F_1$ domain (azide plus PGO) or with the transmembrane $H^+$ pathway within the $F_O$ portion (oligomycin plus PGO or DCCD plus PGO). Briefly, these experiments aimed at clarifying if PGO can combine with the ternary $ESI_1$ complex to form the quaternary $ESI_1I_2$ complex or if the binding of the first inhibitor prevents the binding of the other inhibitor, in other words if the two inhibitors of the $F_1F_O$-ATPase are mutually exclusive. The reciprocal of $Ca^{2+}$- and $Mg^{2+}$-activated $F_1F_O$-ATPase activity in the presence and in the absence of fixed azide concentrations was plotted as a function of increasing PGO concentrations. Two straight lines intersecting above the *x* axis in presence of $Ca^{2+}$ (Fig. 3A) and $Mg^{2+}$ (Fig. 3B) were obtained. This result depicts a simultaneous interaction of PGO and azide with the enzyme. The graphically obtained $\alpha K'_{i2}$ value is the dissociation constant of PGO from the enzyme–substrate–azide complex (*ES*·azide). Similarly, by employing adequate binary mixtures of PGO plus one of the two $F_O$ inhibitors, namely increasing [PGO] and constant [oligomycin] (Fig. 3C,D), and increasing [PGO] and constant [DCCD] (Fig. 3E,F) and evaluating the $Ca^{2+}$- and $Mg^{2+}$-activated $F_1F_O$-ATPase activities, the graphically obtained $\alpha K'_i$ values represent the dissociation constants of the *ES*·oligo·PGO complex and of the *ES*·DCCD·PGO complex, respectively. The $\alpha K'_i$ values of the three binary mixtures tested on the $Ca^{2+}$- and $Mg^{2+}$-activated $F_1F_O$-ATPase are reported in Table 1. The interaction constant (α) between two different compounds bound to the enzyme obtained from the $\alpha K'_i$ to $K'_i$ ratio indicates if the binding of one inhibitor (azide, oligomycin or DCCD) affects ($\alpha \neq 1$) or does not affect ($\alpha = 1$) PGO binding to *ES* (Table 2). Since for the $Ca^{2+}$-activated $F_1F_O$-ATPase all the $F_1$ and $F_O$ inhibitors tested in binary mixtures with PGO $\alpha = 1$ is obtained, the two inhibitors bind independently of each other to yield the $ESI_1I_2$ complex. A different situation is pointed out in the case of the $Mg^{2+}$-activated $F_1F_O$-ATPase. All the calculated α values are > 1, thus indicating that in the presence of inhibitors of $F_1$ or $F_O$ domain PGO binding to the enzyme is somehow hindered.

### 3.3. mPTP sensitivity to PGO

The mPTP activity can be detected by adding $Ca^{2+}$ at subsequent steps to the mitochondrial suspensions and by evaluating the CRC, which represents the capability of intact mitochondria to accumulate $Ca^{2+}$. According to the method employed, the $Ca^{2+}$ release from mitochondria ascribed to mPTP opening is revealed by an increase in fluorescence intensity. In control mitochondria CRC increases upon subsequent 10 µM $Ca^{2+}$ additions at fixed time intervals, as shown by the rise in the (Fura-FF high $Ca^{2+}$)/(Fura-FF low $Ca^{2+}$) ratio, indicated in Fig. 4A as Fura-FF ratio. In the presence of MgADP, mPTP opening is delayed and a higher CRC is detected. Mitochondrial suspensions were treated with 0.5 and 1.0 mM PGO, which correspond to the $IC_{50}$ values for the $Ca^{2+}$- and $Mg^{2+}$-activated $F_1F_O$-ATPases respectively, and with 3.5 mM PGO, namely the concentration that produces the maximal inhibition on the $Ca^{2+}$-activated $F_1F_O$-ATPase. ~~respectively~~, The mPTP opening sensitization to $Ca^{2+}$ can be appreciated by the decrease in CRC, as the rise in fluorescence intensity appears earlier (Fig. 4A), namely at lower PGO concentrations. Consistently, the mPTP formation extent, expressed as ratio of the number of $Ca^{2+}$ pulses required to induce the mPTP in MgADP inhibited ($CRC_i$) and untreated ($CRC_o$) mitochondria, is doubled in the presence of 0.5 and 1.0 mM PGO, while it is apparently unaffected by 3.5 mM PGO (Fig. 4B). Therefore, the ability of PGO to modulate the mPTP in swine heart mitochondria is apparently concentration dependent.

## 4. Discussion

When the $F_1F_O$-ATPase functions as $H^+$ pump by exploiting the free energy of ATP hydrolysis it can use different divalent cations as cofactor [32]. The present findings, obtained on freeze-thawed mitochondria which are clearly permeable to substrates, cofactors and inhibitors, clearly show that PGO more efficiently inhibits the $Ca^{2+}$-activated $F_1F_O$-ATPase than the $Mg^{2+}$-activated $F_1F_O$-ATPase, even if both the differently activated enzyme activities are PGO-susceptive (Fig. 1). Recently, a new role in mitochondrial bioenergetics was ascribed to the $F_1F_O$-ATPase: an energy-dissipating mechanism [33] that, when activated by $Ca^{2+}$, triggers the mPTP formation [21] and is responsible for the reversible mPTP opening. PGO was shown to modulate the mPTP in a species-dependent manner by post-translational modifications of an Arg residue of *g* subunit [6]. The uncompetitive inhibition mechanism of the $F_1F_O$-ATPase with respect to the ATP substrate in presence of either $Ca^{2+}$ or $Mg^{2+}$ shows that PGO does not interact with the enzyme cofactor sites and binds to a different site from that of ATP. Accordingly, the *ES-PGO* complex only forms when the *ES* complex has already been formed (Fig. 2). Multiple inhibition analyses with binary mixtures of PGO and azide, known to block ATP hydrolysis when Pi leaves the catalytic site [34], indicate that ~~since~~ PGO and azide do not mutually exclude and can form the quaternary *ES*·azide·PGO complex (Fig. 3A,B). Therefore, PGO binds to a different site from the azide binding site in the catalytic sites of $F_1$ domain.

In the structurally and functionally coupled $F_1F_O$-ATPase complex the blockage of $H^+$ translocation inhibits ATP hydrolysis. The experiments with the binary mixtures tested, namely oligomycin plus PGO and DCCD plus PGO, show that PGO does not prevent the transmembrane $H^+$ flow within $F_O$. Oligomycin and DCCD bind to the $H^+$ binding sites of *c*-ring and inhibit the $F_1F_O$-ATPase. Differently, PGO binds to the $F_1F_O$-ATPase complex to form the $ESI_1$·PGO complex, without interfering with the binding sites of $F_O$ inhibitors (Fig. 3C,D and 3E,F).

Therefore, PGO binds to the enzyme without interfering in the catalytic mechanism of the $F_1$ domain and in the $H^+$ translocation mechanism of $F_O$ domain. However, the results point out some differences in the response of the two differently activated $F_1F_O$-ATPase activities. On considering the lower $\alpha K'_i$ values of the $Ca^{2+}$-activated $F_1F_O$-ATPase than that of the $Mg^{2+}$-activated $F_1F_O$-ATPase, it is clear that the PGO has a greater propensity to form the quaternary complex ($ESI_1I_2$) in the presence of $Ca^{2+}$ than in the presence of $Mg^{2+}$. Moreover, the α value >1 obtained for the $Mg^{2+}$-activated $F_1F_O$-ATPase with all the inhibitors under study (Table 2) indicates that the inhibitors of $F_1/F_O$ domain and PGO mutually hinder. On the contrary all the α values obtained for the $Ca^{2+}$-activated $F_1F_O$-ATPase are around 1.0, which indicates no interference between the distinct inhibitor binding sites. Since $Mg^{2+}$ and $Ca^{2+}$ insertions are expected to promote different conformational changes on the $F_1F_O$-ATPase [35,36], the more striking PGO inhibition on the $Ca^{2+}$-activated $F_1F_O$-ATPase could be explained by a modification of the enzyme structure caused by Arg adducts. These adducts do not alter ATP binding and $H^+$ translocation mechanism, but apparently make the enzyme more prone to form the mPTP.

In rat mitochondria 1 mM PGO was reported to inhibit the mPTP and to marginally affect the transmembrane potential generation by exploiting ATP hydrolysis in the presence of rotenone [24]. In our experiments, since the $F_1F_O$-ATPase activity rate is only almost halved by a similar PGO concentration ($IC_{50}$= 1.10±0.07 mM), the $F_1F_O$-ATPase may still be able to re-energize the IMM to some extent. Furthermore, the same 1 mM PGO treatment which was reported to 90% inhibit the mPTP in rat liver mitochondria activates the mPTP in swine heart mitochondria (Fig. 4). The $Ca^{2+}$-activated $F_1F_O$-ATPase activity was proven as essential to trigger mPTP opening [21]. However, the $Ca^{2+}$- activated $F_1F_O$-ATPase inhibition by PGO apparently contrasts with ~~and~~ the concomitant PGO-driven facilitation of the mPTP (Fig. 4). This enigma can be tentatively solved on considering a putative structural role of the PGO-modified Arg. Among the many Arg residues of the $F_1F_O$-ATPase, located in α, β, γ, ε subunit of $F_1$ domain, and in *a*, *c* and *g* subunits of $F_O$ domain, apparently the only Arg candidate to form an adduct with PGO responsible of mPTP formation is the conserved Arg-107 of *g* subunit in yeast, which corresponds to Arg-96 in the human sequence [6]. Therefore, the Arg of *g* subunit could represent the PGO modified aminoacid residue. Apparently, such

chemical change results in the $F_1F_O$-ATPase inhibition but does not affect either the $F_1$ catalytic mechanism or $H^+$ translocation within $F_O$ (Fig. 3). Accordingly, the *g* subunit is involved in one of the dimerization sites by combining with the *k* subunit of the adjacent monomer. Moreover it joins the *e* subunit and the N-terminal helix of *b* subunits of each monomer to set up a "BAR-like domain" in the dimer that bends the IMM [7]. It seems likely that the PGO adduct on the *g* subunit may promote a conformational re-arrangement in the transmembrane portion of $F_1F_O$-ATPase supercomplex which mimics the oligomeric $Ca^{2+}$-activated $F_1F_O$-ATPase conformation which forms the mPTP. This structural re-arrangement would prevent the chemo-mechanical coupling of ATP hydrolysis, alter the IMM curvature and the formation of the *cristae* so as to favour the mPTP formation [35].

## 5. Conclusion

Some interesting clues emerge from the present findings. The $F_1F_O$-ATPase catalytic mechanism and the $H^+$ translocation, both activated by $Mg^{2+}$ or by $Ca^{2+}$, even if to a different extent, are indirectly inhibited by PGO, namely the inhibitor, without directly targeting the catalytic sites or the $H^+$ channel, affects the enzyme function. Interestingly, when the $F_1F_O$-ATPase activity is sustained by $Ca^{2+}$ instead of by $Mg^{2+}$, the enzyme activity is more strongly inhibited and mPTP formation is facilitated. Since the enzyme is assumed to have a different conformation when it binds $Ca^{2+}$ or $Mg^{2+}$ [37], PGO binding slightly differs due to the different properties of the activating cation. The apparent discrepancy in the PGO-driven mPTP facilitation accompanied bythe inhibition of the $Ca^{2+}$-activated $F_1F_O$-ATPase activity, strongly implicated in mPTP formation, can be overwhelmed on considering that the Arg adduct may change the $F_1F_O$-ATPase conformation/structure so as to mimic the enzyme steric arrangement involved in the mPTP. Future studies, aiming at enlightening the supramolecular $F_1F_O$-ATPase organization, are expected to add further details to shed light on the structural changes in the enzyme complex and on its relationship with the mPTP. On these bases, the multi-tasking $F_1F_O$-ATPase may emerge as a promising drug binding bioarchitecture to counteract mPTP-related diseases [38].

## Conflicts of interest

No competing interests declared.


## Acknowledgements and funding information

Danilo Matteuzzi (Department of Veterinary Medical Sciences, University of Bologna) is gratefully acknowledged for kindly conferring swine hearts from a local abattoir to our laboratory.

This work was financed by a RFO grant from the University of Bologna, Italy and from the Carisbo Foundation (2018/0375), Bologna, Italy.

## References


[1] N. Mitome, S. Ono, H. Sato, T. Suzuki, N. Sone, M. Yoshida, Essential arginine residue of the F(o)-a subunit in F(o)F(1)-ATP synthase has a role to prevent the proton shortcut without c-ring rotation in the F(o) proton channel, Biochem. J. 430 (2010) 171–177. https://doi.org/10.1042/BJ20100621.

[2] L. Langemeyer, S. Engelbrecht, Essential arginine in subunit a and aspartate in subunit c of FoF1 ATP synthase: effect of repositioning within helix 4 of subunit a and helix 2 of subunit c, Biochim. Biophys. Acta. 1767 (2007) 998–1005. https://doi.org/10.1016/j.bbabio.2007.05.007.

[3] W. Junge, H. Lill, S. Engelbrecht, ATP synthase: An electrochemical transducer with rotatory mechanics, Trends in Biochemical Sciences. 22 (1997) 420–423. https://doi.org/10.1016/S0968-0004(97)01129-8.

[4] P. Paumard, J. Vaillier, B. Coulary, J. Schaeffer, V. Soubannier, D.M. Mueller, D. Brèthes, J.-P. di Rago, J. Velours, The ATP synthase is involved in generating mitochondrial cristae morphology, EMBO J. 21 (2002) 221–230. https://doi.org/10.1093/emboj/21.3.221.

[5] L. Guo, M. Carraro, A. Carrer, G. Minervini, A. Urbani, I. Masgras, S.C.E. Tosatto, I. Szabò, P. Bernardi, G. Lippe, Arg-8 of yeast subunit e contributes to the stability of F-ATP synthase dimers and to the generation of the full-conductance mitochondrial megachannel, J. Biol. Chem. 294 (2019) 10987–10997. https://doi.org/10.1074/jbc.RA119.008775.

[6] L. Guo, M. Carraro, G. Sartori, G. Minervini, O. Eriksson, V. Petronilli, P. Bernardi, Arginine 107 of yeast ATP synthase subunit g mediates sensitivity of the mitochondrial permeability transition to phenylglyoxal, J. Biol. Chem. 293 (2018) 14632–14645. https://doi.org/10.1074/jbc.RA118.004495.

[7] J. Gu, L. Zhang, S. Zong, R. Guo, T. Liu, J. Yi, P. Wang, W. Zhuo, M. Yang, Cryo-EM structure of the mammalian ATP synthase tetramer bound with inhibitory protein IF1, Science. 364 (2019) 1068–1075. https://doi.org/10.1126/science.aaw4852.

[8] P.D. Boyer, The ATP synthase--a splendid molecular machine, Annu. Rev. Biochem. 66 (1997) 717–749. https://doi.org/10.1146/annurev.biochem.66.1.717.

[9] P.D. Boyer, Catalytic site occupancy during ATP synthase catalysis, FEBS Lett. 512 (2002) 29–32. https://doi.org/10.1016/S0014-5793(02)02293-7.

[10] S. Nesci, F. Trombetti, V. Ventrella, A. Pagliarani, Opposite rotation directions in the synthesis and hydrolysis of ATP by the ATP synthase: hints from a subunit asymmetry, J. Membr. Biol. 248 (2015) 163–169. https://doi.org/10.1007/s00232-014-9760-y.

[11] H. Guo, S.A. Bueler, J.L. Rubinstein, Atomic model for the dimeric FO region of mitochondrial ATP synthase, Science. 358 (2017) 936–940. https://doi.org/10.1126/science.aao4815.

[12] S. Nesci, A. Pagliarani, Emerging Roles for the Mitochondrial ATP Synthase Supercomplexes, Trends Biochem. Sci. 44 (2019) 821–823. https://doi.org/10.1016/j.tibs.2019.07.002.

[13] M. Carraro, V. Checchetto, G. Sartori, R. Kucharczyk, J.-P. di Rago, G. Minervini, C. Franchin, G. Arrigoni, V. Giorgio, V. Petronilli, S.C.E. Tosatto, G. Lippe, I. Szabó, P. Bernardi, High-Conductance Channel Formation in Yeast Mitochondria is Mediated by F-ATP Synthase e and g Subunits, Cell. Physiol. Biochem. 50 (2018) 1840–1855. https://doi.org/10.1159/000494864.

[14] V. Giorgio, S. von Stockum, M. Antoniel, A. Fabbro, F. Fogolari, M. Forte, G.D. Glick, V. Petronilli, M. Zoratti, I. Szabó, G. Lippe, P. Bernardi, Dimers of mitochondrial ATP synthase form the permeability transition pore, Proc. Natl. Acad. Sci. U.S.A. 110 (2013) 5887–5892. https://doi.org/10.1073/pnas.1217823110.

[15] M. Bonora, A. Bononi, E. De Marchi, C. Giorgi, M. Lebiedzinska, S. Marchi, S. Patergnani, A. Rimessi, J.M. Suski, A. Wojtala, M.R. Wieckowski, G. Kroemer, L. Galluzzi, P. Pinton, Role of the c subunit of the FO ATP synthase in mitochondrial permeability transition, Cell Cycle. 12 (2013) 674–683. https://doi.org/10.4161/cc.23599.

[16] K.N. Alavian, G. Beutner, E. Lazrove, S. Sacchetti, H.-A. Park, P. Licznerski, H. Li, P. Nabili, K. Hockensmith, M. Graham, G.A. Porter, E.A. Jonas, An uncoupling channel within the c-subunit ring of the F1FO ATP synthase is the mitochondrial permeability transition pore, Proc. Natl. Acad. Sci. U.S.A. 111 (2014) 10580–10585. https://doi.org/10.1073/pnas.1401591111.

[17] J. Carroll, J. He, S. Ding, I.M. Fearnley, J.E. Walker, Persistence of the permeability transition pore in human mitochondria devoid of an assembled ATP synthase, Proc. Natl. Acad. Sci. U.S.A. 116 (2019) 12816–12821. https://doi.org/10.1073/pnas.1904005116.
[18] S. Nesci, F. Trombetti, C. Algieri, A. Pagliarani, A Therapeutic Role for the F1FO-ATP Synthase, SLAS Discov. 24 (2019) 893–903. https://doi.org/10.1177/2472555219860448.
[19] N. Jiang, H. Bo, C. Song, J. Guo, F. Zhao, H. Feng, H. Ding, L. Ji, Y. Zhang, Increased vulnerability with aging to MPTP: the mechanisms underlying mitochondrial dynamics, Neurol. Res. 36 (2014) 722–732. https://doi.org/10.1179/1743132813Y.0000000296.
[20] M.A. Neginskaya, M.E. Solesio, E.V. Berezhnaya, G.F. Amodeo, N. Mnatsakanyan, E.A. Jonas, E.V. Pavlov, ATP Synthase C-Subunit-Deficient Mitochondria Have a Small Cyclosporine A-Sensitive Channel, but Lack the Permeability Transition Pore, Cell Rep. 26 (2019) 11-17.e2. https://doi.org/10.1016/j.celrep.2018.12.033.
[21] C. Algieri, F. Trobetti, A. Pagliarani, V. Ventrella, C. Bernardini, M. Fabbri, M. Forni, S. Nesci, The mitochondrial Ca2+-activated $F_1F_O$-ATPase hydrolyses ATP and promotes the permeability transition pore, Annals of the New York Academy of Sciences. (2019). https://doi.org/10.1111/nyas.14218.
[22] K. Takahashi, The reactions of phenylglyoxal and related reagents with amino acids, J. Biochem. 81 (1977) 395–402. https://doi.org/10.1093/oxfordjournals.jbchem.a131471.
[23] M.D. Linder, S. Morkunaite-Haimi, P.K.J. Kinnunen, P. Bernardi, O. Eriksson, Ligand-selective modulation of the permeability transition pore by arginine modification. Opposing effects of p-hydroxyphenylglyoxal and phenylglyoxal, J. Biol. Chem. 277 (2002) 937–942. https://doi.org/10.1074/jbc.M107610200.
[24] O. Eriksson, E. Fontaine, P. Bernardi, Chemical modification of arginines by 2,3-butanedione and phenylglyoxal causes closure of the mitochondrial permeability transition pore, J. Biol. Chem. 273 (1998) 12669–12674. https://doi.org/10.1074/jbc.273.20.12669.
[25] M. Johans, E. Milanesi, M. Franck, C. Johans, J. Liobikas, M. Panagiotaki, L. Greci, G. Principato, P.K.J. Kinnunen, P. Bernardi, P. Costantini, O. Eriksson, Modification of permeability transition pore arginine(s) by phenylglyoxal derivatives in isolated mitochondria and mammalian cells. Structure-function relationship of arginine ligands, J. Biol. Chem. 280 (2005) 12130–12136. https://doi.org/10.1074/jbc.M413454200.
[26] S. Nesci, V. Ventrella, F. Trombetti, M. Pirini, A. Pagliarani, The mitochondrial F1FO-ATPase desensitization to oligomycin by tributyltin is due to thiol oxidation, Biochimie. 97 (2014) 128–137. https://doi.org/10.1016/j.biochi.2013.10.002.
[27] M.M. Bradford, A rapid and sensitive method for the quantitation of microgram quantities of protein utilizing the principle of protein-dye binding, Anal. Biochem. 72 (1976) 248–254. https://doi.org/10.1006/abio.1976.9999.
[28] V. Ventrella, S. Nesci, F. Trombetti, P. Bandiera, M. Pirini, A.R. Borgatti, A. Pagliarani, Tributyltin inhibits the oligomycin-sensitive Mg-ATPase activity in Mytilus galloprovincialis digestive gland mitochondria, Comp. Biochem. Physiol. C Toxicol. Pharmacol. 153 (2011) 75–81. https://doi.org/10.1016/j.cbpc.2010.08.007.
[29] A. Cornish-Bowden, A simple graphical method for determining the inhibition constants of mixed, uncompetitive and non-competitive inhibitors, Biochem. J. 137 (1974) 143–144. https://doi.org/10.1042/bj1370143.
[30] T. Yonetani, The Yonetani-Theorell graphical method for examining overlapping subsites of enzyme active centers, Meth. Enzymol. 87 (1982) 500–509. https://doi.org/10.1016/s0076-6879(82)87028-6.
[31] S. Nesci, V. Ventrella, F. Trombetti, M. Pirini, A. Pagliarani, Thiol oxidation is crucial in the desensitization of the mitochondrial F1FO-ATPase to oligomycin and other macrolide antibiotics, Biochim. Biophys. Acta. 1840 (2014) 1882–1891. https://doi.org/10.1016/j.bbagen.2014.01.008.
[32] S. Nesci, F. Trombetti, V. Ventrella, M. Pirini, A. Pagliarani, Kinetic properties of the mitochondrial F1FO-ATPase activity elicited by Ca(2+) in replacement of Mg(2+), Biochimie. 140 (2017) 73–81. https://doi.org/10.1016/j.biochi.2017.06.013.
[33] P. Bernardi, A. Rasola, M. Forte, G. Lippe, The Mitochondrial Permeability Transition Pore: Channel Formation by F-ATP Synthase, Integration in Signal Transduction, and Role in Pathophysiology, Physiol. Rev. 95 (2015) 1111–1155. https://doi.org/10.1152/physrev.00001.2015.

[34] D. Bald, T. Amano, E. Muneyuki, B. Pitard, J.L. Rigaud, J. Kruip, T. Hisabori, M. Yoshida, M. Shibata, ATP synthesis by F0F1-ATP synthase independent of noncatalytic nucleotide binding sites and insensitive to azide inhibition, J. Biol. Chem. 273 (1998) 865–870. https://doi.org/10.1074/jbc.273.2.865.
[35] S. Nesci, F. Trombetti, V. Ventrella, A. Pagliarani, From the Ca2+-activated F1FO-ATPase to the mitochondrial permeability transition pore: an overview, Biochimie. 152 (2018) 85–93. https://doi.org/10.1016/j.biochi.2018.06.022.
[36] S. Nesci, New insight in a new entity: the mitochondrial permeability transition pore arises from the Ca2+-activated F1FO-ATPases, Science Bulletin. 63 (2018) 143–145. https://doi.org/10.1016/j.scib.2017.12.019.
[37] V. Giorgio, V. Burchell, M. Schiavone, C. Bassot, G. Minervini, V. Petronilli, F. Argenton, M. Forte, S. Tosatto, G. Lippe, P. Bernardi, Ca(2+) binding to F-ATP synthase β subunit triggers the mitochondrial permeability transition, EMBO Rep. 18 (2017) 1065–1076. https://doi.org/10.15252/embr.201643354.
[38] S. Nesci, The mitochondrial permeability transition pore in cell death: A promising drug binding bioarchitecture, Medicinal Research Reviews. (2019) 1–7. https://doi.org/10.1002/med.21635.

## Figure Legends

Figure 1. Dose-response curve of PGO on the $F_1F_O$-ATPase activity. $Ca^{2+}$-activated $F_1F_O$-ATPase (▲) and $Mg^{2+}$-activated $F_1F_O$-ATPase activities (Δ) in the presence of increasing PGO concentrations. Data represent the mean ± SD from three independent experiments carried out on distinct mitochondrial preparations.

Figure 2. Mitochondrial $F_1F_O$-ATPase inhibition by PGO. Dixon (A, C) and Cornish–Bowden (B, D) plots obtained at 1 mM (○) or 3 mM (●) ATP for the $Ca^{2+}$-activated $F_1F_O$-ATPase (A,B); 3 mM (□) or 6 mM (■) ATP for the $Mg^{2+}$-$F_1F_O$-activated ATPase (C, D) and designing the experiments as detailed in Section 2.4. All points represent the mean ± SD (vertical bars) of four distinct experiments carried out on distinct mitochondrial preparations.

Figure 3. Multiple inhibitor analysis by Dixon plots for the mitochondrial $F_1F_O$-ATPase inhibition by PGO. The F-ATPase assay, in the presence of 2 mM $Ca^{2+}$ plus 3 mM ATP (A, C, E) and in presence of 2 mM $Mg^{2+}$ plus 6 mM ATP (B, D, F) were carried out in the absence (○) or in the presence of 25 μM azide(●); in the absence (Δ) or in the presence of 3 μg/mL oligomycin (▲); in the absence (□) or in the presence of 0.25 μM DCCD (■), as detailed in Section 2.4. Each point represents the mean value ± SD (vertical bars) of at least three experiments carried out on distinct mitochondrial preparations.

Figure 4. Evaluation of mPTP opening. Representative curves (A) of the calcium retention capacity (CRC) expressed as Fura-FF ratio, monitored in response to subsequent 10 μM $CaCl_2$ pulses (shown by the triangles), as detailed in Section 2.5, in untreated mitochondria (Control), and in the presence of 2 mM MgADP, 0.5, 1.0 or 3.5 mM PGO. B) Quantitation of the mPTP is expressed as the ratio of the number of calcium pulses required to induce the mPTP in MgADP inhibited ($CRC_i$) and untreated ($CRC_o$) mitochondria. Data represent the mean ± SD from three independent experiments carried out on distinct mitochondrial preparations. * indicates significant differences with respect to the control ($P \leq 0.05$).

Legend to Graphical Abstract. $Ca^{2+}$ induces the enzyme conformation which opens the mitochondrial permeability transition pore (mPTP). Phenylglyoxal (PGO) inhibits the $F_1F_O$-ATPase activity either activated by $Ca^{2+}$ or by $Mg^{2+}$, but favours the enzyme conformation which opens the mPTP in the presence of $Ca^{2+}$.

## Tables

Table 1. Dissociation constant ($\alpha K'_{i2}$) of the quaternary complex $ESI_1I_2$ of PGO ($I_1$) with each of the inhibitors ($I_2$): azide ($F_1$ inhibitor) and oligomycin (oligo) or DCCD ($F_O$ inhibitors).

| $ESI_1 + I_2$ | $\alpha K'_{i2}$ (mM) | | | | | |
|---|---|---|---|---|---|---|
| | $Ca^{2+}$-ATPase | | | $Mg^{2+}$-ATPase | | |
| *ES* azide + PGO | 0.69 | ± | 0.04 | 1.17 | ± | 0.09 |
| *ES* oligo + PGO | 0.70 | ± | 0.05 | 1.21 | ± | 0.11 |
| *ES* DCCD + PGO | 0.61 | ± | 0.06 | 1.26 | ± | 0.10 |

$\alpha K'_{i2}$ values were graphically obtained from the Dixon plots of Fig. 3 as detailed in the section 2.4. Data are the mean ± SD of three different experiment carried out on different mitochondrial pools.

Table 2. Interaction constants (α) between PGO ($I_2$) and the inhibitors ($I_1$): azide on the $F_1$ domain and oligomycin or DCCD on the $F_O$ domain in the $ESI_1I_2$ complex formation.

| | Azide | Oligomycin | DCCD | |
|---|---|---|---|---|
| PGO | 1.08 | 1.09 | 0.95 | $Ca^{2+}$-activated $F_1F_O$-ATPase |
| | 1.43 | 1.48 | 1.54 | $Mg^{2+}$-activated $F_1F_O$-ATPase |

α values were obtained as detailed in Section 3.2. Data are the mean ± SD of three different experiments carried out on different mitochondrial pools.

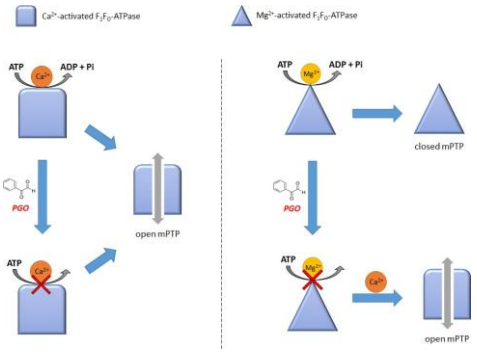
Ca2+-activated F1F0-ATPase
Mg2+-activated F1F0-ATPase
ATP
ADP + Pi
Ca2+
Mg2+
PGO
open mPTP
closed mPTP

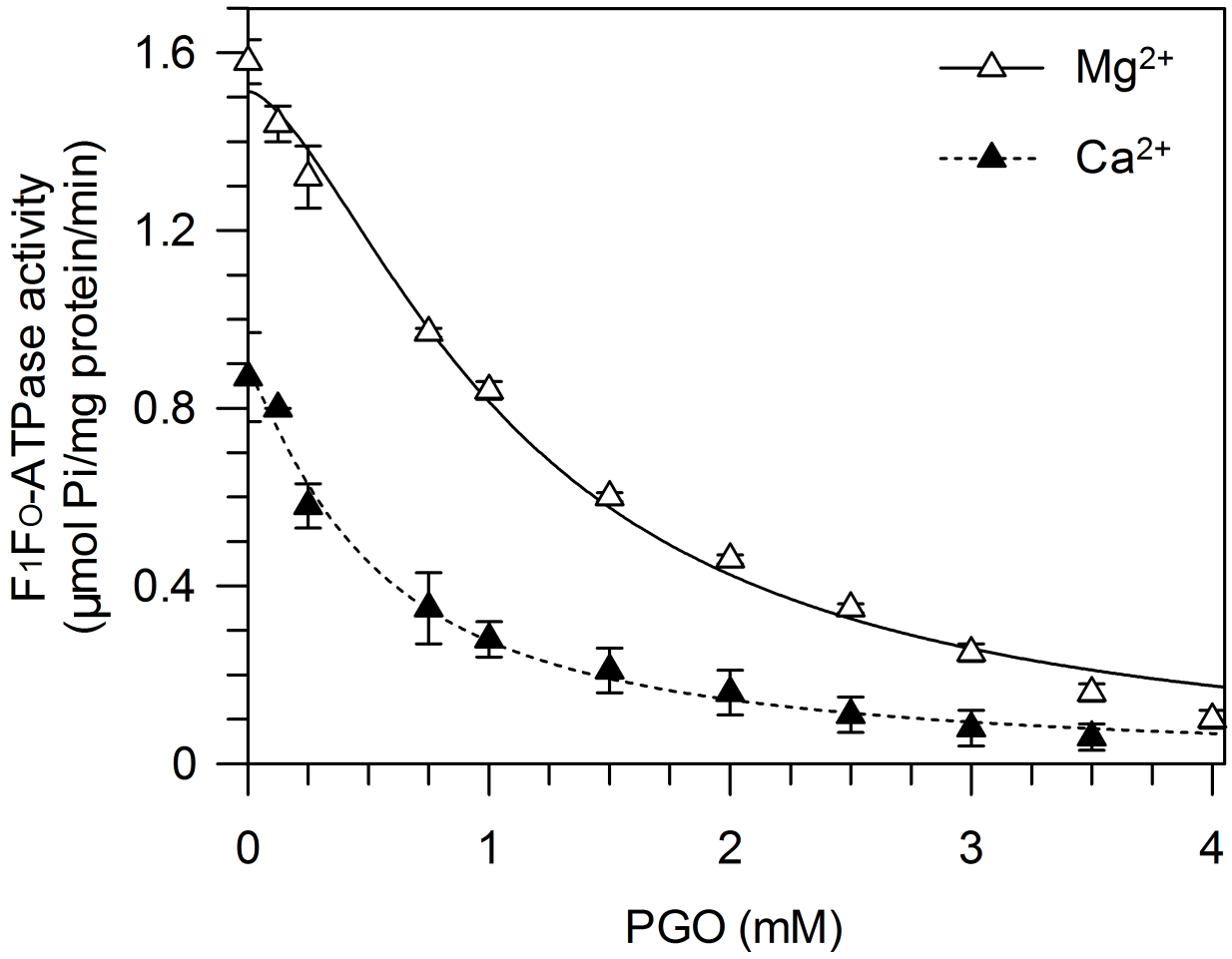
1.6
1.2
0.8
0.4
0
0
1
2
3
4
F1FO-ATPase activity
(µmol Pi/mg protein/min)
PGO (mM)
Mg2+
Ca2+

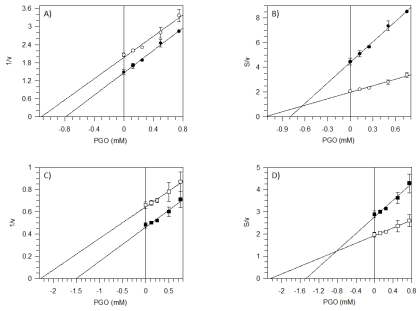
A)
1/v
PGO (mM)
B)
S/v
PGO (mM)
C)
1/v
PGO (mM)
D)
S/v
PGO (mM)

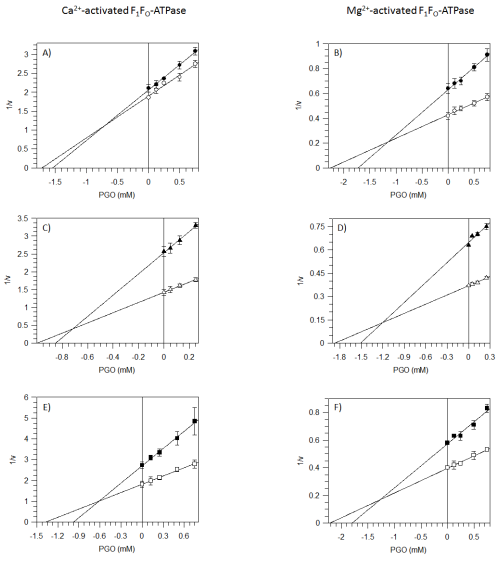
Ca2+-activated F1FO-ATPase
Mg2+-activated F1FO-ATPase
A)
B)
C)
D)
E)
F)
1/v
PGO (mM)

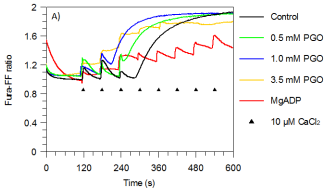
A)
Fura-FF ratio
Time (s)
Control
0.5 mM PGO
1.0 mM PGO
3.5 mM PGO
MgADP
10 µM CaCl2

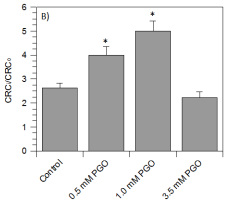
B)
CRC/CRC50
Control
0.5 mM PGO
1.0 mM PGO
3.5 mM PGO